Enzymatic starch hydrolysis performance of Taylor-Couette flow reactor with ribbed inner cylinder

Matsumoto, Masahiro ; Masuda, Hayato ; Hubacz, Robert ; Horie, Takafumi ; Iyota, Hiroyuki ; Shimoyamada, Makoto ; Ohmura, Naoto

(Citation)
Chemical Engineering Science,231:116270

(Issue Date)
2021-02-15

(Resource Type)
journal article

(Version)
Accepted Manuscript

Title:

Enzymatic starch hydrolysis performance of Taylor–Couette flow reactor with ribbed inner cylinder

Authors:

Masahiro Matsumoto[a], Hayato Masuda[a, b, c]*, Robert Hubacz[d], Takafumi Horie[c, e], Hiroyuki Iyota[b], Makoto Shimoyamada[a], Naoto Ohmura[c, e]

Affiliation:

[a] School of Food and Nutritional Science, University of Shizuoka, 52-1 Yada, Suruga-ku, Shizuoka 422-8526, Japan

[b] Department of Mechanical and Physical Engineering, Osaka City University, 3-3-138 Sugimoto, Sumiyoshi-ku, Osaka 558-8585, Japan

[c] Complex Fluid and Thermal Engineering Research Center (COFTEC), Kobe University, 1-1 Rokkodai, Nada-ku, Kobe, Hyogo 657-8501, Japan

[d] Warsaw University of Technology, Faculty of Chemical and Process Engineering, ul. Waryńskiego 1, 00-645 Warszawa, Poland

[e] Department of Chemical Science and Engineering, Kobe University, 1-1 Rokkodai,

Nada-ku, Kobe, Hyogo 657-8501, Japan

Corresponding author:

* To whom corresponded should be addressed:

E-mail address: hayato-masuda@eng.osaka-cu.ac.jp

Highlights

- A Taylor–Couette flow reactor is applied to a continuous starch hydrolysis process.
- A sufficient reducing sugar yield is obtained in the Taylor vortex flow regime.
- A ribbed inner cylinder suppresses axial dispersion caused by the wavy motion of Taylor cells.
- A ribbed inner cylinder enhances the starch hydrolysis process.

Keywords: Taylor–Couette flow reactor; Process intensification; Starch hydrolysis process; Ribbed inner cylinder; Viscosity change; Mixing enhancement

Abstract

In this study, a Taylor–Couette flow reactor (TCFR) was applied to starch hydrolysis accompanied with an intricate viscosity change during reaction for the purpose of process intensification. In industries, several reactors are used in starch hydrolysis, namely gelatinization, liquefaction, and saccharification. It was possible to conduct a continuous starch hydrolysis with one TCFR. In addition, a sufficient reducing sugar yield was obtained in the Taylor vortex flow regime. However, the yield decreased at a higher effective Reynolds number (Re_{eff}) due to axial dispersion through a bypass flow generated by the wavy motion of Taylor cells. In order to immobilize Taylor vortex flow at this condition, a ribbed inner cylinder was employed which suppressed axial dispersion at the higher Re_{eff}. As a result, a higher reducing sugar yield was successfully obtained than that by using a standard cylinder, demonstrating that the optimization of TCFR geometry has the potential for process intensification.

1. Introduction

Recent challenges concerning the environment, energy and increasing population have heightened demand for new technologies directed at saving energy and spaces and promoting a healthy environment, among other objectives. Chemical industries have particularly focused on process intensification (PI) to address these challenges. According to Stankiewicz (2000), PI involves the development of novel apparatuses and techniques that, compared with those typically used today, are expected to advance dramatic improvements in manufacturing and processing by substantially decreasing the equipment size/production capacity ratio, energy consumption, or waste production, and ultimately resulting in less expensive, sustainable technologies.

Reay et al. (2013) offers two reactor design strategies for achieving PI: enhancement of transport rates (momentum, heat and mass), and applying the same processing experience to every molecule. Another effective PI approach is the "conversion from batch to continuous operation" because continuous reactors are typically smaller than equivalent batch reactors (Boodhoo and Harvey, 2013). Such approaches indicate that a continuous reactor with sufficient transport rates and a narrow residence time distribution (RTD) is required to achieve PI. One such reactor is the Taylor–Couette flow reactor (TCFR). Taylor–Couette flow is the flow between coaxial cylinders with

the inner cylinder rotating. Taylor (1923) initially discovered that counter-rotating toroidal vortices spaced regularly along the axis are generated when the Reynolds number (Re) in the circumference exceeds the critical Re (Re_{cr}). The toroidal motion enhances mixing and heat/mass transfer. In addition, all the fluid elements leaving the reactor have the same residence time when a relatively small axial flow is added (Kataoka et al., 1975). Furthermore, compared with the conventional stirred tank reactor, there is no region where the locally strong shear force is imposed. This is beneficial to processes employing shear-sensitive materials. To take advantage of these features, TCFR has been applied to various processes, e.g., emulsion polymerization (Kataoka et al., 1995), particle synthesis (Ogihara et al., 1995), photocatalytic reaction (Sczechowski et al., 1995; Dutta and Ray, 2004), enzymatic reaction (Giordano et al., 2000), bioprocess (Qiao et al., 2018) and reverse osmosis process (Lee and Lueptow, 2001), and recently, to food processes such as heat sterilization of liquid food (Forney et al., 2004; Orlowska et al., 2014; Masuda et al., 2017c; Masuda et al., 2019a, 2019b) and production of textured soy-bean meat replacers (Krintiras et al., 2016).

In order to establish PI using continuous reactors like TCFR, it is necessary to face how to consider a spatial distribution of physical quantities (e.g. density, temperature and viscosity) caused by chemical reactions. For example, in polymerization or

fermentation process, the viscosity increases with the reaction (Kaminoyama et al., 1997; Potumarthi et al., 2007). The change in viscosity significantly affects the fluid flow, heat/mass transfer and, consequently, the reaction performance. To investigate the possibility of PI using TCFR in the process with complicated viscosity change during the reaction, Masuda et al. (2013, 2017a) applied TCFR to enzymatic hydrolysis process of starch (biopolymer). Starch hydrolysis consists of gelatinization, liquefaction, and saccharification. As shown in Fig. 1, the viscosity intricately changes during these processes. The viscosity of starch suspension significantly increases during gelatinization. Besides, gelatinized starch shows the strong shear-thinning property. When an enzyme is added to the gelatinized starch, the viscosity decreases rapidly and breaks down into reducing sugars. From a practical viewpoint, one of the most severe points is this viscosity change. In addition, the mixing function required is different in each process. Gelatinization requires heat transfer and dispersion of starch particles. Liquefaction and saccharification require highly efficient mixing, as a small amount of enzyme is added to highly viscous gelatinized starch, and also must avoid the excess shear force to ensure the enzyme activity. Thus, the current starch hydrolysis process employs several apparatuses, resulting in a massive total size (Baruque Filho et al., 2000). Conversely, it is possible to conduct continuous starch hydrolysis using one

TCFR due to the enhanced characteristics of mixing and heat/mass transfer. Masuda et al. (2013, 2017a) successfully showed that a higher reducing sugar yield was obtained in the Taylor vortex flow regime. However, the yield decreased at a higher *Re*, presumably induced by axial dispersion caused by the wavy motion of Taylor vortex flow. The enhanced mixing condition at a higher *Re* would be desirable for decomposition of starch into sugar having a smaller molecular such as glucose or maltose. In addition, Masuda et al. (2017a) changed the diameter of the inner cylinder between gelatinization and liquefaction/saccharification, which demonstrated that shape modification of the inner cylinder has potential for the mixing enhancement of Taylor vortex flow. Other research also explored the optimization of the inner cylinder shape (Soos et al., 2007; Sorg et al., 2011). In particular, Richter et al. (2008, 2009) found that a ribbed inner cylinder stabilized the structure of Taylor vortex flow at a higher Re. This research confirmed that a ribbed inner cylinder suppresses axial dispersion even in the wavy Taylor vortex flow regime, while enhancing mixing in Taylor cells. Applying a ribbed cylinder to the starch hydrolysis process can achieve further intensification due to the stabilization of the structure of Taylor vortices.

This study aims to intensify the starch hydrolysis process using TCFR with a ribbed inner cylinder. Based on the RTD and the reducing sugar yield, performance using the

ribbed inner cylinder was compared to that using a standard inner cylinder. As discussed, the intricate change in the viscosity during starch hydrolysis complicates the flow condition in the apparatus. Therefore, to preliminarily investigate the effect of the ribbed inner cylinder on the performance, dextrin hydrolysis, in which there is no viscosity change during reaction, was selected as a model reaction. It is noted that dextrin solution is generally a low viscous Newtonian fluid. Next, based on the results of the dextrin hydrolysis experiments, starch hydrolysis experiments were performed.

2. Materials and Methods

2.1. Experimental apparatus

The Taylor–Couette flow reactor (TCFR) used in this study consisted of a rotating inner cylinder (the outer radius (R_i): 12.5 mm) and a stationary outer cylinder (the inner radius (R_o): 17.5 mm), as shown in Fig. 2. The length of the cylinders (L) and the gap width (d) were 300 mm and 5 mm, respectively. The angular velocity of the inner cylinder, ω, was varied from 2.5 to 50 rad/s. The starch or dextrin suspension at room temperature was introduced from the inlet. The axial velocity, u, was varied from 0.145 to 0.418 mm/s. The initial concentration of starch suspension or dextrin solution, C_0, was 250 g/L. For the starch hydrolysis experiments, α–amylase derived from *Bacillus*

licheniformis (Termamyl 120L, Novozymes) was injected at the middle point of TCFR. For the dextrin hydrolysis experiments, the injection point was 50 mm from the inlet. Thus, it should be noted that the enzyme injection point is different between each experiment. The volumetric flow rate of the enzyme, v_e, was varied from 0.1 to 1.5 mL/h. Two water jackets were included to control temperature during processing. For the starch hydrolysis experiments, two jackets were set to 85°C. For the dextrin hydrolysis experiments, two jackets were set to 65°C. Two types of inner cylinders, standard and ribbed, were used. Figure 3 depicts the ribbed cylinder schematically. The distance between each cell, d_{cell} (= 2d), was 10 mm, indicating that the pair of vortices was segmented by ribs. The width of the ribs was 2.5 mm. The height of the ribs, h_{rib}, was 2.5 and 4.5 mm as shown in Fig. 4. To optimize rib configuration in the inner cylinder, the length of the ribbed section from the outlet, L_{rib} in Fig. 2, were varied. In the dextrin hydrolysis experiments, ribs were equipped downstream along the axis (L_{rib} = 250 mm). In contrast to the dextrin solution, the starch hydrolysis experiments involved highly viscous fluids. In such systems, channeling or sedimentation would typically occur around ribs. To avoid this undesirable condition, ribs should be located in the section where the viscosity relatively decreases due to the liquefaction reaction. Thus, in the starch hydrolysis experiments, L_{rib} was set to 50 to 100 mm.

2.2. Sample handling and analysis

Product samples were taken from the outlet of the apparatus at $\theta = 2.5$. θ means the normalized time as follows:

$$\theta = \frac{u(R_o^2 - R_i^2)\pi \cdot t}{V_r} \#(1)$$

According to Kataoka et al. (1995), the conversion of a chemical reaction reaches a steady-state value after $\theta = 2$ in a TCFR. Thus, the sampling at $\theta = 2.5$ is adequate to investigate the performance of TCFR.

To halt the liquefaction reaction, samples were immediately cooled to approximately 0°C and their pH was reduced to 2 by the addition of HCl. The sample was centrifuged at 15,000 G for 2,400 s to separate the solid and liquid phases. To measure the liquefaction rate (*LR*) (i.e. the ratio of the liquid phase weight (W_{liquid}) to the total weight of the sample (W_{total})), the solid phase (W_{solid}) was weighed. The value of *LR* was calculated as follows:

$$LR = W_{liquid}/W_{total} = (W_{total} - W_{solid})/W_{total} \#(2)$$

The carbohydrate composition and the reducing sugar concentration in the liquid phase of sample were also investigated. The carbohydrate composition was analyzed using a high performance liquid chromatography (HPLC). The HPLC column (Asahipak,

NH2P-50, Shodex®) having the inner diameter of 4.6 mm and the length of 250 mm was used with acetic acid in water (30%, v/v) as the mobile phase at 0.4 mL/min. The concentration of glucose, maltose and maltotriose in the liquid phase was quantified. Besides, the total concentration of reducing sugar in the liquid phase of sample, C_{rs}, was measured by the dinitro salicylic acid (DNS) method. Adding the DNS reagent, the sample reagent colors the sample and allows analyzing the reducing sugar concentration using a UV-VIS spectrophotometer (V-630, JASCO Corp.) at a wavelength of 540 nm.

Each experiment was repeated more than three times. Only one sample was measured and analyzed. The average values are shown in each figure.

2.3. Residence time distribution (RTD) measurements

To understand the characteristics of axial dispersion, the residence time distribution (RTD) was measured using a salt-solution technique. The working fluid was an aqueous solution of 25wt% concentration of glycerin. The tracer was 200 g/L concentration of a NaCl solution. The 1 mL tracer was impulsively injected from the injection port which is located at 50 mm from the inlet. This means the actual length of TCFR in the tracer response experiments was 250 mm. The electric conductivity of the effluent was measured using an electric conductivity meter (CM-42X, DDK-TOA Corp.). The

measurement was converted to the tracer concentration from a calibration curve. The RTD was obtained by normalizing the tracer concentration, E_θ, with the normalized time (θ) as follows (Richter et al., 2008):

$$E_\theta = \frac{V_\mathrm{r} \cdot C(t)}{u(R_\mathrm{o}^2 - R_\mathrm{i}^2)\pi \cdot \int_0^\infty C(t)\,\mathrm{d}t} \#(3)$$

2.4. Definition of the effective Reynolds number (Re_{eff})

The flow pattern of Taylor vortex flow is characterized by *Re*, which is defined as follows:

$$Re = \frac{\rho\omega R_\mathrm{i} d}{\eta} \#(4)$$

where ρ [kg/m^3] is the fluid density, ω [rad/s] is the angular velocity of the inner cylinder, and η [Pa·s] is the fluid viscosity. Calculating *Re* for the starch hydrolysis reaction is more difficult. The viscosity decreases with the hydrolysis reaction. According to Masuda et al. (2017a), the drastic decrease in viscosity is observed only in the initial stage of the reaction, i.e., the rheological properties of the effluent can be regarded as the representative properties for the calculation of *Re*. Another challenge is the spatial change in viscosity due to the shear-thinning property of polysaccharide solutions. As Ohta et al. (2003, 2005) suggested, in non-Newtonian fluid systems, the construction of the effective Reynolds number, Re_{eff}, based on the effective viscosity

(η_{eff}), is necessary from a practical perspective. To properly determine η_{eff}, the method of estimating the effective shear-rate, γ_{eff}, should be considered. For a Taylor–Couette flow system, Masuda et al. (2017b) proposed an empirical correlation for the estimation of γ_{eff} from the angular velocity of the inner cylinder, ω, as follows:

$$\gamma_{\mathrm{eff}} = \left\{77.05n^{0.32}\left(\frac{R_{\mathrm{i}}}{R_{\mathrm{o}}}\right)^{2} - 88.73n^{0.31}\left(\frac{R_{\mathrm{i}}}{R_{\mathrm{o}}}\right) + 26.85n^{0.21}\right\}\cdot\omega \#(5)$$

The value of n is a model parameter in the Carreau model (1972), which is the rheological model used in this study:

$$\eta = \eta_0[1 + (\beta\cdot\dot{\gamma})^2]^{\frac{(n-1)}{2}} \#(6)$$

where η_0 is the zero shear-rate viscosity, $\dot{\gamma}$ is the shear-rate and β is the characteristic time. It can be obtained by applying the rheological property of the effluent to the Carreau model (Eq. (6)). Equation (5) estimates the value of γ_{eff} is estimated from ω and n. Consequently, Re_{eff} can be estimated from η_{eff} which is calculated by substituting γ_{eff} for $\dot{\gamma}$ in the Carreau model (Eq. (6)).

3. Results and Discussion

3.1. Dextrin hydrolysis process

Figure 5 illustrates the dependence of the reducing sugar yield C_{rs}/C_0 on Re and u in the dextrin hydrolysis process. According to Taylor (1923), the theoretical Re_{cr} without

axial flow is 82.2 for the radius ratio R_i/R_o = 0.714 of the TCFR used. Strictly speaking, Re_{cr} depends on the axial Reynolds number, Re_{ax}, which is defined as follows (Lueptow et al., 1992):

$$Re_{ax} = \frac{\rho u(2d)}{\eta} \#(7)$$

The maximum value of Re_{ax} within the experimental conditions was about 2.0. According to Lueptow et al. (1992), such low value of Re_{ax} does not affect Re_{cr}.

In Fig. 5, in all cases of u, higher C_{rs}/C_0 was obtained above Re_{cr} (= 82.2), indicating the enhancement of mixing and heat transfer due to Taylor vortex flow improved the hydrolysis reaction of dextrin. However, in all cases of u, C_{rs}/C_0 slightly decreased above approximately Re = 900. Although higher shear force at a higher Re would induce inactivation of α–amylase (van der Veen et al., 2004), such extremely high shear force is not imposed in TCFR. In starch hydrolysis system, Masuda et al. (2013, 2017a) also reported the decrease in the reducing sugar yield at a higher Re, and explained this was due to the wavy motion of Taylor vortices which affects TCFR performance as a reactor because mass diffusion over cell boundaries (intermixing) is enhanced and the injection fluid (enzyme) would diffuse through a bypass flow caused by this wavy motion (Ohmura et al., 1997; Wereley and Lueptow, 1999).

According to Richter et al. (2008), using a ribbed inner cylinder is effective to

suppress the wavy motion even at a higher *Re*. Figure 6 shows the flow visualization at *Re* = 905.1 (a) without rib and (b) with ribs (h_{rib} = 4.5 mm). In flow visualization experiments, it should be noted that an aqueous solution of 25wt% glycerin was used and no axial flow was imposed. The flow was visualized by adding small amount of Iriodin® (Iriodin® silver-white pigment, MERCK) to the glycerin solutions. This substance consists of small, light reflecting slabs, which arrange themselves along streamlines due to the viscous forces (Richter et al., 2008). As shown in Fig. 6 (a), dark streaks correspond to the inflow boundary wave in the case of no rib. This wavy motion causes intermixing and bypass diffusion. As a result, axial dispersion is induced. Conversely, in the case of ribbed inner cylinder, a pair of vortices is segmented and immobilized by the rib (Fig. 6 (b)). Thus, axial dispersion is expected to be suppressed even the wavy Taylor vortex flow regime. In order to investigate the cross-sectional structure of Taylor vortices, numerical simulation was conducted based on the method reported (Masuda et al., 2017b). The density and viscosity of aqueous solution of 25wt% glycerin was used for the simulation. Figure 7 shows the cross-sectional view of velocity field at *Re* = 905.1 (a) without rib and (b) with ribs (h_{rib} = 4.5 mm). It should be noted the aspect ratio in the simulation differed from the experimental condition. As shown in Fig. 7, the suppression of wavy motion at the inflow boundary was also

confirmed.

In order to clarify the characteristics of TCFR with or without ribs, RTD (E_θ curve) at Re = 905.1 and Re_{ax} = 2.0 was investigated as shown in Fig. 8. The fitting lines based on the tanks-in-series model (Eq. (8)) were also drawn (Levenspiel, 1999):

$$E_\theta = \frac{N}{(N-1)!}(N\theta)^{N-1}\exp(-N\theta) \#(8)$$

where N [–] is the number of tanks in series. In the case of no rib (h_{rib} = 0 mm), the RTD similar to a continuous stirred tank reactor (CSTR) model was obtained. Although the RTD at h_{rib} = 2.5 mm becomes marginally sharp compared with the standard inner cylinder, there was no clear effect of ribs on the suppression of axial dispersion. Remarkably, the sharp RTD, i.e., plug flow type RTD, was obtained at h_{rib} = 4.5 mm due to the robust immobilization and stabilization of Taylor vortices. The values of N, which is obtained by fitting Eq. (8) to the experimental results (RTD), were 2 (no rib), 4 (h_{rib} = 2.5 mm), and 17 (h_{rib} = 4.5 mm), respectively. In the tracer response experiments, 25 pairs of vortices are ideally formed. Because one pair of vortices is regarded as one stirred vessel (Ohmura et al., 1997), the ideal value of N with no axial dispersion is 25. Thus, it was found the RTD at h_{rib} = 4.5 mm close approaches the ideal condition.

The degree of axial dispersion was evaluated based on the dispersion coefficient (**D**). The differential equation representing the dispersion model is as follows:

$$\frac{\partial C}{\partial \theta} = \left(\frac{\mathbf{D}}{uL}\right)\frac{\partial^2 C}{\partial z^2} - \frac{\partial C}{\partial z} \#(9)$$

where the dimensionless group (**D** / *uL*), called the vessel dispersion number, is the parameter that measures the extent of axial dispersion (Levenspiel, 1999). By numerically solving Eq. (9) using the results of tracer response experiments, the dispersion number was estimated. The dispersion number in TCFR with or without ribs is shown in Fig. 9. In the case of h_{rib} / d = 0.9 (i.e. h_{rib} = 4.5 mm), the significantly low dispersion number was successfully obtained and it is closely to the value in the ideal cascade of 25 stirred vessels (the dotted line in Fig. 9). Thus, the rib with h_{rib} = 4.5 mm was used for the dextrin/starch hydrolysis experiments.

Figure 10 illustrates the effect of the ribbed inner cylinder on C_{rs}/C_0 at u = 0.418 mm/s in the dextrin hydrolysis experiment. As expected, the ribbed inner cylinder suppressed the decrease in C_{rs}/C_0 at a higher *Re*. In addition, using the ribbed inner cylinder, the sufficient C_{rs}/C_0 was obtained at a relatively low *Re*. In the case of ribbed inner cylinder, as shown in Fig. 4, a pair of vortices (Ekman cells) between ribs is formed even below Re_{cr} due to Ekman boundary layers (Czamy et al., 2003). Therefore, the ribbed inner cylinder is expected to improve mixing at a lower *Re* and suppress axial dispersion at a higher *Re*.

3.2. Starch hydrolysis process

Figure 11 depicts the dependence of the liquefaction rate (LR) on Re_{eff} at u = 0.418 mm/s in the standard and ribbed inner cylinders (h_{rib} = 4.5 mm). In the case of ribbed inner cylinder, two types of the length of ribbed section from the outlet (L_{rib}) was investigated. In the Taylor vortex flow region, starch liquefaction was conducted sufficiently and continuously in both cylinders. In the standard inner cylinder, the LR increased with the increase in Re_{eff}. In contrast, the ribbed cylinder largely exhibited no dependence of LR on Re_{eff}. Remarkably, higher LR was obtained even at a relatively low Re_{eff} when employing the ribbed inner cylinder. As described in the previous section, it is considered that pairs of vortices between ribs enhanced mixing of gelatinized starch and enzyme.

Figure 12 shows the dependence of C_{rs}/C_0 on Re_{eff} at u = 0.418 mm/s in the standard and ribbed inner cylinders in the starch hydrolysis process. For the standard inner cylinder, the decrease in C_{rs}/C_0 at a higher Re_{eff} was observed, although a high value of C_{rs}/C_0 was obtained in the Taylor vortex flow regime. For the ribbed inner cylinder, there was no decrease in C_{rs}/C_0 at a higher Re_{eff}. On the contrary, at L_{rib} = 50 mm, C_{rs}/C_0 slightly increased with the increase in Re_{eff} even above Re_{eff} = 1,000. Therefore, it is considered that the ribbed inner cylinder suppresses axial dispersion at a higher Re_{eff}

1 even in the starch hydrolysis process. In another case where L_{rib} = 100 mm, C_{rs}/C_0
2 remained constant with an increase in Re_{eff}, indicating that in this case a sufficient
3 mixing condition for starch hydrolysis was achieved even at low Re_{eff}.

4 Figure 13 illustrates the dependence of the yield of small saccharides, C_{ss}/C_0, on
5 Re_{eff} at u = 0.418 mm/s with the standard and ribbed inner cylinders in starch hydrolysis
6 process. C_{ss} is the concentration of small saccharides and is calculated as follow:

$$C_{ss} = C_g + C_m + C_{mt} \#(10)$$

7 where C_g, C_m and C_{mt} are the concentration of glucose, maltose, and maltotriose,
8 respectively. As evident in Fig. 13, above Re_{eff} = 500, a significantly higher value of
9 C_{ss}/C_0 was obtained using the ribbed inner cylinder compared with that using the
10 standard inner cylinder. Thus, it was determined that a mixing enhancement suppressing
11 axial dispersion using the ribbed inner cylinder further intensifies the starch hydrolysis
12 process.

13 As with the result of C_{rs}/C_0 shown in Fig. 12, the dependence of C_{ss}/C_0 on Re_{eff}
14 differed between L_{rib} = 50 and 100 mm. From a practical perspective, Re_{eff} and L_{rib}
15 should be optimized. For example, Fig. 13 indicates that the comparable value of C_{ss}/C_0
16 was obtained in Re_{eff} = 397, L_{rib} = 50 mm and Re_{eff} = 91, L_{rib} = 100 mm. In general,
17 increasing the number of ribs equipped would increase power consumption. Therefore,

Re_{eff} = 397, L_{rib} = 50 mm appears to be a more efficient condition than Re_{eff} = 91, L_{rib} = 100 mm. However, a higher Re_{eff} condition naturally requires higher power consumption. Therefore, in order to optimize starch hydrolysis using the ribbed inner cylinder, it is necessary to investigate power consumption at each condition. Besides, the optimization of h_{rib} is also beneficial for process design in the future. Nevertheless, it can be concluded that the ribbed inner cylinder is effective for the production of small saccharides even in relatively high starch concentration system.

4. Conclusions

A Taylor–Couette flow reactor (TCFR) was applied to dextrin and starch hydrolysis processes to achieve process intensification. In both processes, the reducing sugar yield increased in the Taylor vortex flow region, because the toroidal motion of Taylor vortices enhanced the mixing of substrates with an enzyme. However, the yield decreased at a higher Reynolds number (Re) and effective Reynolds number (Re_{eff}). The residence time distribution (RTD) was broad at a higher Re in the tracer response experiment. Thus, it was determined that the axial dispersion induced by the wavy motion of Taylor cells at higher Re and Re_{eff} caused the decrease in the reducing sugar yield.

In order to immobilize Taylor cells at a higher *Re*, a ribbed inner cylinder was used. A relatively sharp RTD was obtained using this cylinder. Because the ribbed inner cylinder suppressed axial dispersion, there was no decrease in the reducing sugar yield at higher *Re* and Re_{eff}. Furthermore, in the starch hydrolysis process, a significantly higher yield of small saccharides was obtained using the ribbed inner cylinder compared than that using the standard inner cylinder.

Acknowledgements

This research was partially supported by the Ministry of Education, Science, Sports and Culture of Japan, Grant-in-Aid for Scientific Research (A), (No. 18H03853), and Fund for the Promotion of Joint International Research (Fostering Joint International Research (B)), (No. 19KK0127), from the Japan Society for the Promotion of Science (JSPS). This study was also financially supported by The Food Science Institute Foundation.

Nomenclature

E_θ	normalized tracer concentration, –
C	concentration, g/L
C_g	glucose concentration, g/L
C_m	maltose concentration, g/L
C_{mt}	maltotriose concentration, g/L
C_{rs}	reducing sugar concentration, g/L
C_{ss}	small saccharide concentration, g/L
C_0	initial concentration of substrate, g/L
$\mathbf{D}_z$	dispersion coefficient, m^2/s
d	gap width, mm
d_{cell}	distance between each cell, mm
E_θ	normalized tracer concentration, –

1	h_{rib}	height of ribs, mm
2	L	length of cylinders, mm
3	LR	liquefaction rate, –
4	L_{rib}	length of ribbed section from outlet, mm
5	N	number of tanks, –
6	n	model parameter in Carreau model, -
7	u	axial velocity, mm/s
8	v_e	volumetric flow rate of enzyme, mL/h
9	Re	Reynolds number, –
10	Re_{ax}	axial Reynolds number, –
11	Re_{cr}	critical Reynolds number, –
12	Re_{eff}	effective Reynolds number, –
13	R_i	inner cylinder radius, mm
14	R_o	outer cylinder radius, mm
15	t	time, s
16	V_r	reactor volume, mL
17	W_{liquid}	liquid phase weight, g
18	W_{solid}	solid phase weight, g

W_{total} total weight, g

z axial position, mm

Greek letters

β characteristic time, s

$\dot{\gamma}$ shear-rate, 1/s

$\dot{\gamma}_{eff}$ effective shear-rate, 1/s

η viscosity, Pa·s

η_{eff} effective viscosity, Pa·s

θ normalized time, –

ρ density, kg/m^3

ω angular velocity of inner cylinder, rad/s

References

Baruque Filho, E. A., Baroque, M. G. A., Sant'Anna Jr., G. L., 2000. Babassu coconut starch liquefaction: An industrial scale approach to improve conversion yield, Biores. Technol. 75, 49–55.

Boodhoo, K. V. K., Harvey, A., 2013. Process Intensification for green chemistry: Engineering solutions for sustainable chemical processing, John Wiley, Sons.

Carreau, P. J., 1972. Rheological equations from molecular network theories, Trans. Soc. Rheol. 16, 99–127.

Czamy, O., Serre, E., Bontoux, P., 2003. Interaction between Ekman pumping and the centrifugal instability in Taylor–Couette flow, Phys. Fluids, 15, 467–477.

Dutta, P. K., Ray, A. K., 2004. Experimental investigation of Taylor vortex photocatalytic reactor for water purification, Chem. Eng. Sci. 59, 5249–5259.

Forney, L. J., Pierson, J. A., Ye, Z., 2004. Juice irradiation with Taylor–Couette flow:

UV inactivation of *Escherichia coli*, J. Food Protection 67, 2410–2415.

Giordano, R. L. C., Giordano, R. C., Cooney, C. L., 2000. Performance of a continuous Taylor–Couette–Poiseuille vortex flow enzymic reactor with suspended particles, Process Biochem. 35, 1093–1101.

Kaminoyama, M., Nishimura, K., Nishi, K., Kamiwano, M., 1997. Numerical analysis of bulk thermal styrene polymerization in stirred vessel with double helical ribbon impeller, Kagaku Kougaku Ronbunshu 23, 835–843.

Kataoka, K., Doi, H., Kongo, T., Futagawa, M., 1975. Ideal plug-flow properties of Taylor vortex flow, J. Chem. Eng. Japan 8, 472–476.

Kataoka, K., Ohmura, N., Kouzu, M., Simamura, Y., Okubo, M., 1995. Emulsion polymerization of styrene in a continuous Taylor vortex flow reactor, Chem. Eng. Sci. 50, 1409–1416.

Krintiras, G. A., Diaz, J. G., van der Goot, A. J., Stankiewicz, A. I., Stefanidis, G. D., 2016. On the use of the Couette Cell technology for large scale production of textured soy-based meat replacers, J. Food Eng. 169, 205–213.

Lee, S., Lueptow, R. M., 2001. Rotating reverse osmosis: A dynamic model for flux and rejection, J. Memb. Sci. 192, 129–143.

Levenspiel, O., 1999. Chemical reaction engineering, 3rd ed., Jonh Wiley & Sons Inc.

Lueptow, R. M., Docter, A., Min, K., 1992. Stability of axial flow in an annulus with a rotating inner cylinder, Phys. Fluids A, 4, 2446–2455.

Masuda, H., Horie, T., Hubacz, R., Ohmura, N., 2013. Process intensification of continuous starch hydrolysis with a Couette–Taylor flow reactor, Chem. Eng. Res. Design 91, 2259–2264.

Masuda, H., Horie, T., Hubacz, R., Ohmura, N., Shimoyamada, M., 2017a. Process development of starch hydrolysis using mixing characteristics of Taylor vortices, Biosci. Biotechnol. Biochem. 81, 755–761.

Masuda, H., Horie, T., Hubacz, R., Ohta, M., Ohmura, N., 2017b. Prediction of onset of Taylor–Couette instability for shear-thinning fluids, Rheol. Acta 56, 73–84.

Masuda, H., Horie, T., Ohmura, N., Shimoyamada, M., 2017c. Intensification of heat sterilization process for liquid foods using Taylor–Couette flow system, Chem. Eng. Trans. 57, 1753–1758.

Masuda, H., Hubacz, R., Shimoyamada, M., Ohmura, N., 2019a. Numerical simulations of sterilization processes for shear-thinning food in Taylor–Couette flow system, Chem. Eng. Technol. 42, 859–866.

Masuda, H., Hubacz, R., Ohmura, N., Shimoyamada, M., 2019b. Effect of rheological properties of liquid foods on heat sterilization process in Taylor–Couette flow apparatus,

Chem. Eng. Trans. 75, 31–36.

Ogihara, T., Matsuda, G., Yanagawa, T., Ogata, N., Fujita, K., Nomura, M., 1995. Continuous synthesis of monodispersed silica particles using Couette–Taylor vortex flow, J. Ceram. Soc. Japan, 103, 151–154.

Ohmura, N., Kataoka, K., Shibata, Y., Makino, T., 1997. Effective mass diffusion over cell boundaries in a Taylor-Couette flow system, Chem. Eng. Sci., 52, 1757-1765.

Ohta, M., Iwasaki, E., Obata, E., Yoshida, Y., 2003. A numerical study of the motion of a spherical drop rising in shear-thinning fluid systems, J. Non-Newtonian Fluid Mech. 116, 95–111.

Ohta, M., Iwasaki, E., Obata, E., Yoshida, Y., 2005. Dynamic processes in a deformed drop rising through shear-thinning fluids, J. Non-Newtonian Fluid Mech. 132, 100–107.

Orlowska, M., Koutchma, T., Kostrzynska, M., Tang, J., Defelice, C., 2014. Evaluation of mixing flow conditions to inactivate *Escherichia coli* in opaque liquids using pilot-scale Taylor–Couette UV unit, J. Food. Eng. 120, 100–109.

Potumarthi, R., Ch., S., Jetty, A., 2007. Alkaline protease production by submerged fermentation in stirred tank reactor using *Bacillus licheniformis* NCIM-2042: Effect of aeration and agitation regimes, Biochem. Eng. J. 34, 185–192.

Qiao, J., Yan, W. -C., Teoh, J. H., Tong, Y. W., Wang, C. -H., 2018. Experimental and

computational studies of oxygen transport in a Taylor-Couette bioreactor, Chem. Eng. J. 334, 1954–1964.

Reay, D. A., Ramshaw, C., Harvey, A., 2013. Process intensification for green chemistry: Engineering solutions for efficiency, sustainability, and flexibility, 2nd ed., Butterworth-Heinemann, Oxford.

Richter, O., Hoffmann, H., Kraushaar-Czarnetzki, B., 2008. Effect of the rotor shape on the mixing characteristics of a continuous flow Taylor-vortex reactor, Chem. Eng. Sci. 63, 3504–3513.

Richter, O., Menges, M., Kraushaar-Czarnetzki, B., 2009. Investigation of mixing in a rotor shape modified Taylor-vortex reactor by the means of a chemical test reaction, Chem. Eng. Sci. 64, 2384-2391.

Sczechowski, J. G., Koval, C. A., Noble, R. D., 1995. A Taylor vortex reactor for heterogeneous photocatalysis, Chem. Eng. Sci. 50, 3163–3173.

Soos, M., Wu, H., Morbidelli, M., 2007. Taylor–Couette unit with a lobed inner cylinder cross section, AIChE J. 53, 1109–1120.

Sorg, R., Tanzeglock, T., Soos, M., Morbidelli, M., Périlleux, A., Solacroup, T., Broly, H., 2011. Minimizing hydrodynamics stress in mammalian cell culture through the lobed Taylor–Couette bioreactor, Biotechnol. J. 6, 1504–1515.

Stankiewicz, A., Moulijn, J. A., 2000. Process intensification: Transforming chemical engineering. Chem. Eng. Prog. 96, 22–34.

Taylor, G. I., 1923. Stability of a viscous liquid contained between two rotating cylinders, Phil. Trans. Roy. Soc. A. 223, 289–343.

van der Veen, M. E., Van Iersel, D. G., van der Goot, A. J., Boom, R. M., 2004. Shear-induced inactivation of α-amylase in a plain shear field, Biotechnol. Prog., 20, 1140–1145.

Wereley, S. T., Lueptow, R. M., 1999. Velocity field for Taylor–Couette flow with an axial flow, Phys. Fluids, 11, 3637–3649.

Fig. 1. Intricate change of rheological properties during starch hydrolysis.

Fig. 2. Taylor–Couette flow reactor.

Fig. 3. Picture of ribbed inner cylinder.

Fig. 4. Cross-sectional view of a pair of Taylor vortices between ribs.

Fig. 5. Dependence of C_{rs} / C_0 on Re at various u and C_0 = 250 g/L in dextrin hydrolysis experiments. The results in this figure were obtained using the standard inner cylinder. The solid line shows Re_{cr} = 82.2.

Fig. 6. Flow visualization of Taylor–Couette flow with (a) standard and (b) ribbed inner cylinder (h_{rib} = 4.5 mm) at Re = 905.1. An aqueous solution of 25wt% glycerin with small amount of Iriodin® was used for flow visualization experiments.

Fig. 7. Cross-sectional view of velocity field obtained using numerical simulation with (a) standard and (b) ribbed inner cylinder (h_{rib} = 4.5 mm) at Re = 905.1. The density and

viscosity of aqueous solution of 25wt% glycerin was used.

Fig. 8. RTD in TCFR with each cylinder at Re = 905.1 and u = 0.418 mm/s. Solid lines (fitting lines) correspond to tank-in-series model lines. An aqueous solution of 25wt% glycerin was used as the working fluid.

Fig. 9. Effect of normalized rib height (h_{rib} / d) on dispersion number at Re = 905.1 and u = 0.418 mm/s.

Fig. 10. Dependence of C_{rs} / C_0 on Re with standard and ribbed inner cylinder at u = 0.145 mm/s in dextrin hydrolysis experiments.

Fig. 11. Effect of Re_{eff} on LR with three types of cylinders (L_{rib} = 0, 50, 100 mm) at u = 0.240 mm/s in starch hydrolysis experiments.

Fig. 12. Effect of Re_{eff} on C_{rs} / C_0 with three types of cylinders (L_{rib} = 0, 50, 100 mm) at u = 0.240 mm/s in starch hydrolysis experiments.

Fig. 13. Effect of C_{ss} / C_0 on LR with three types of cylinders (L_{rib} = 0, 50, 100 mm) at u = 0.240 mm/s in starch hydrolysis experiments.

Figure1
Click here to download high resolution image

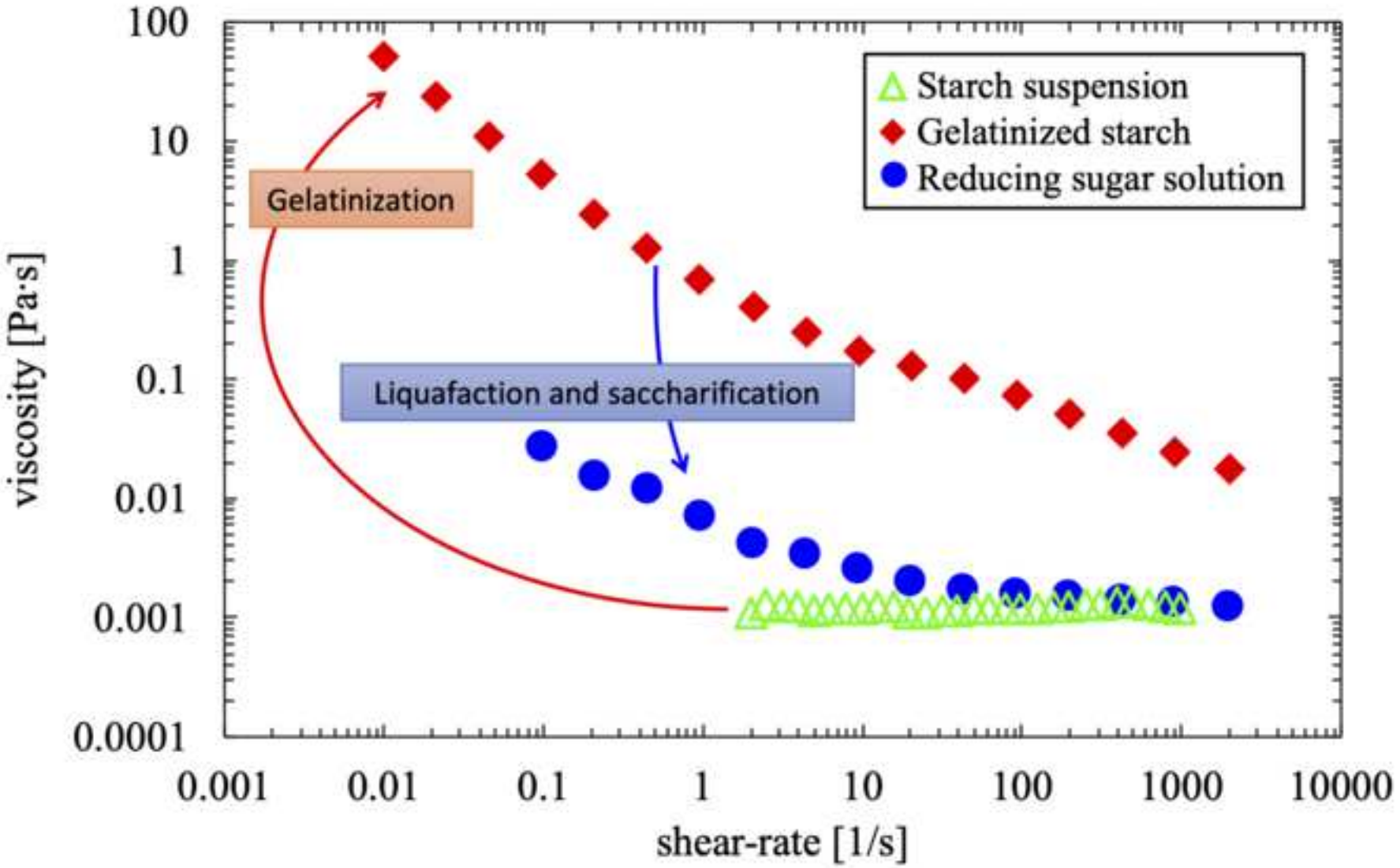

Figure2
Click here to download high resolution image

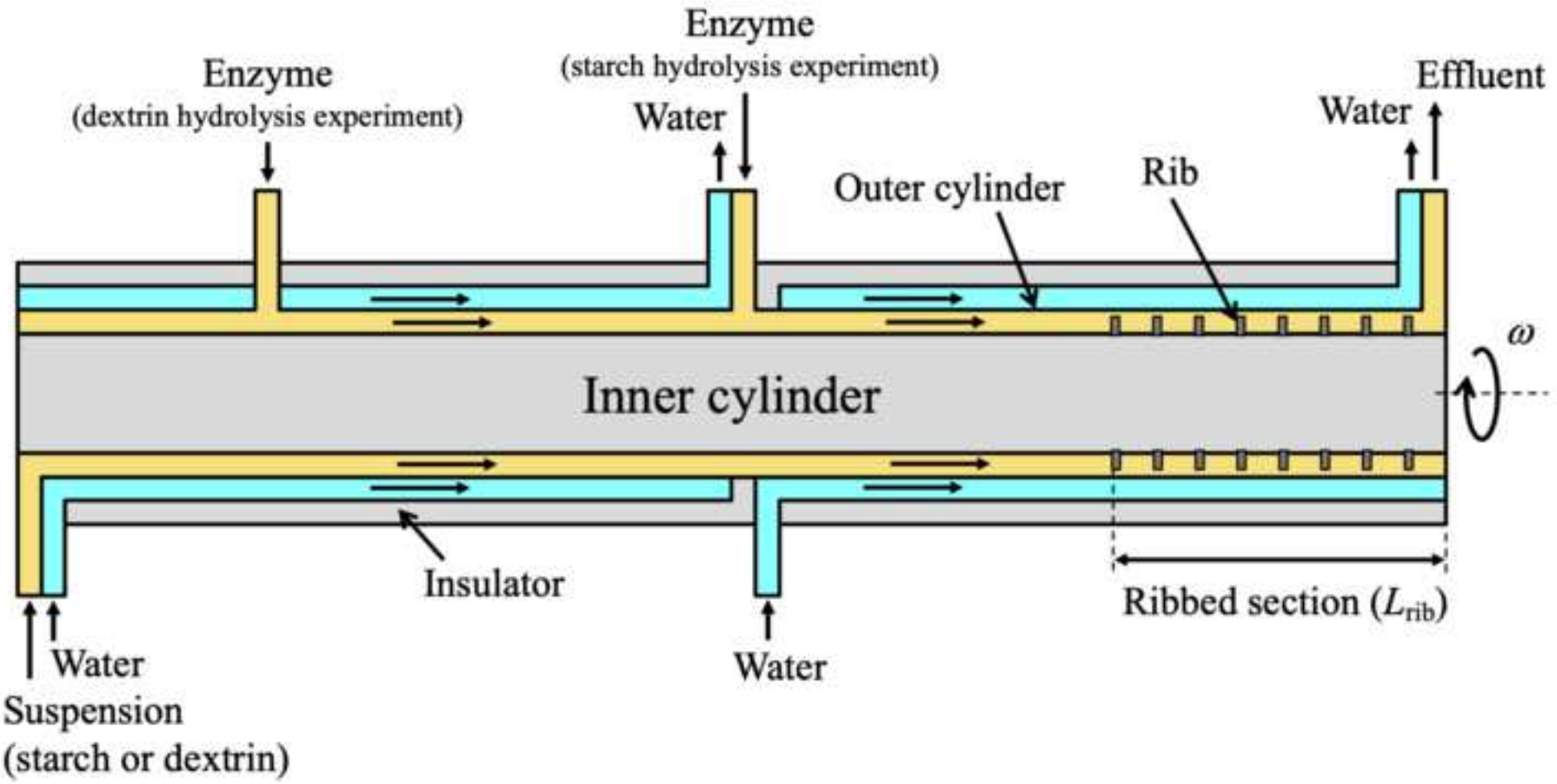

Figure3

Click here to download high resolution image

Figure4
Click here to download high resolution image

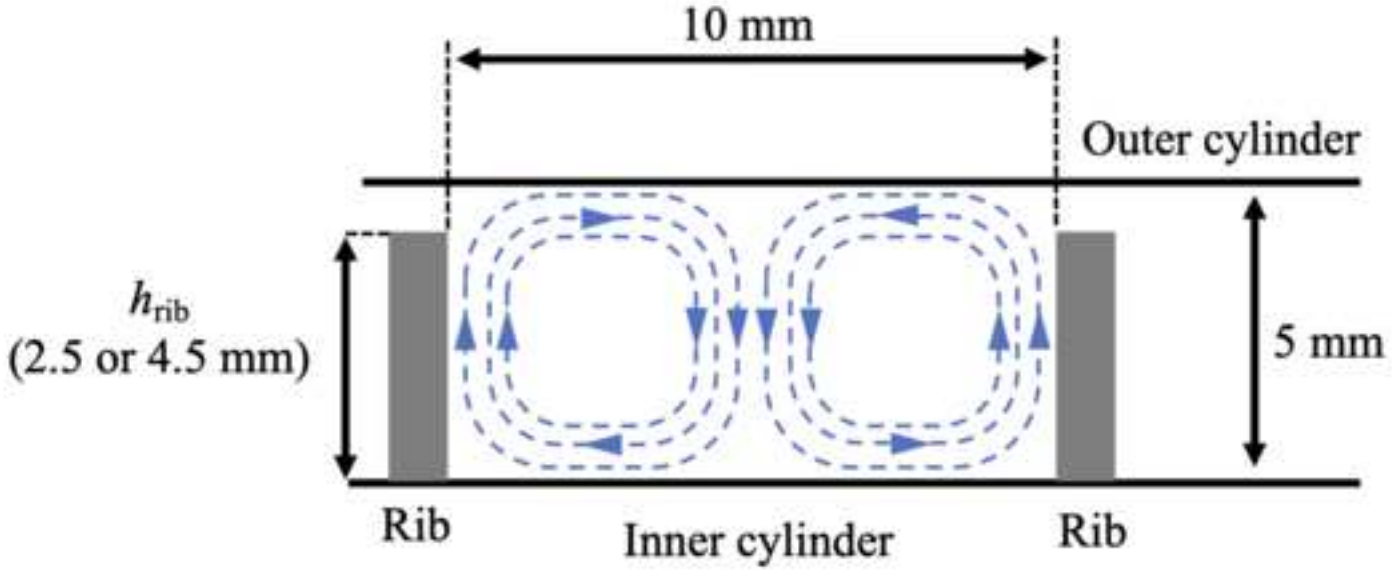

Figure5
Click here to download high resolution image

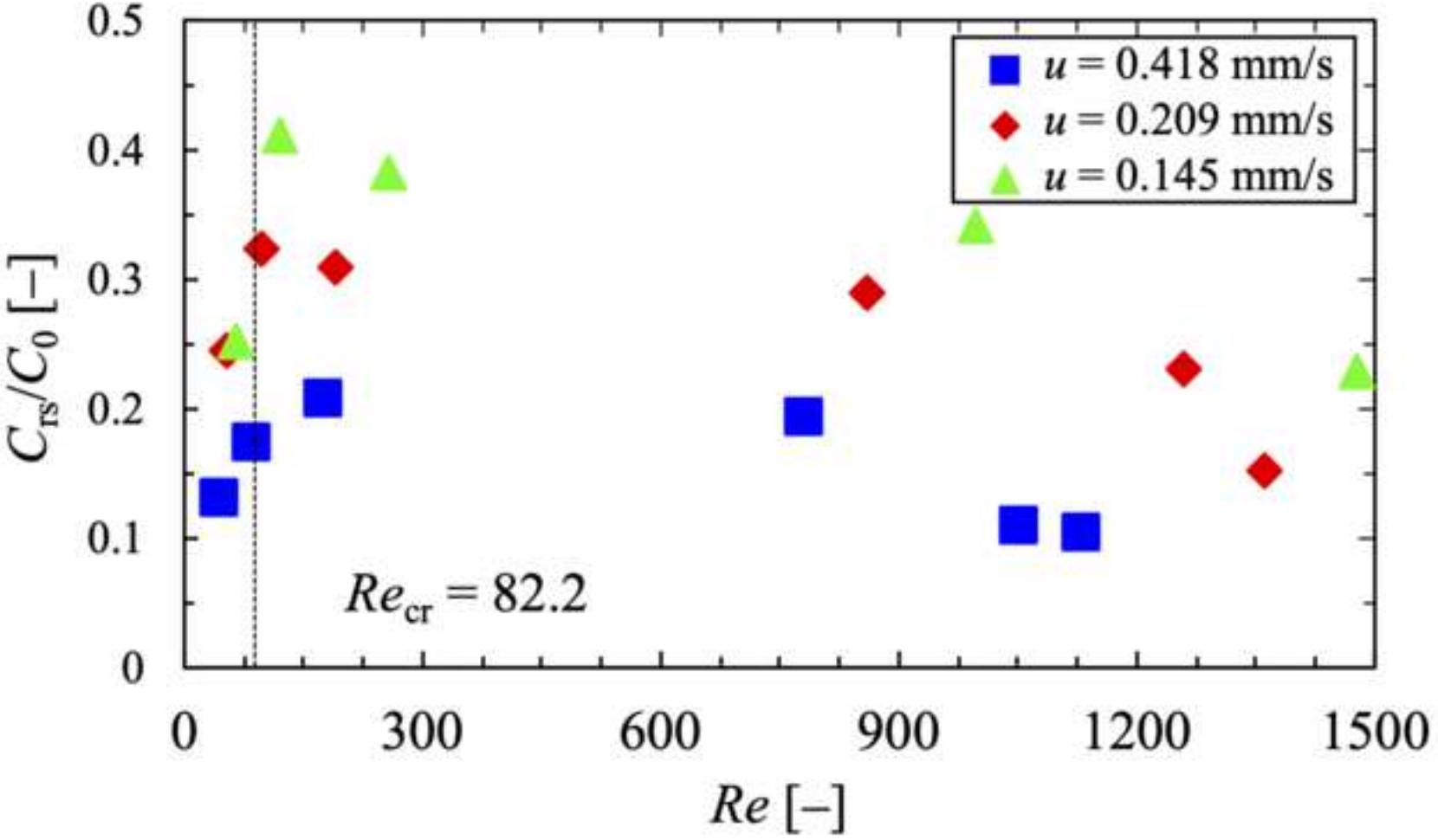

Figure6
Click here to download high resolution image

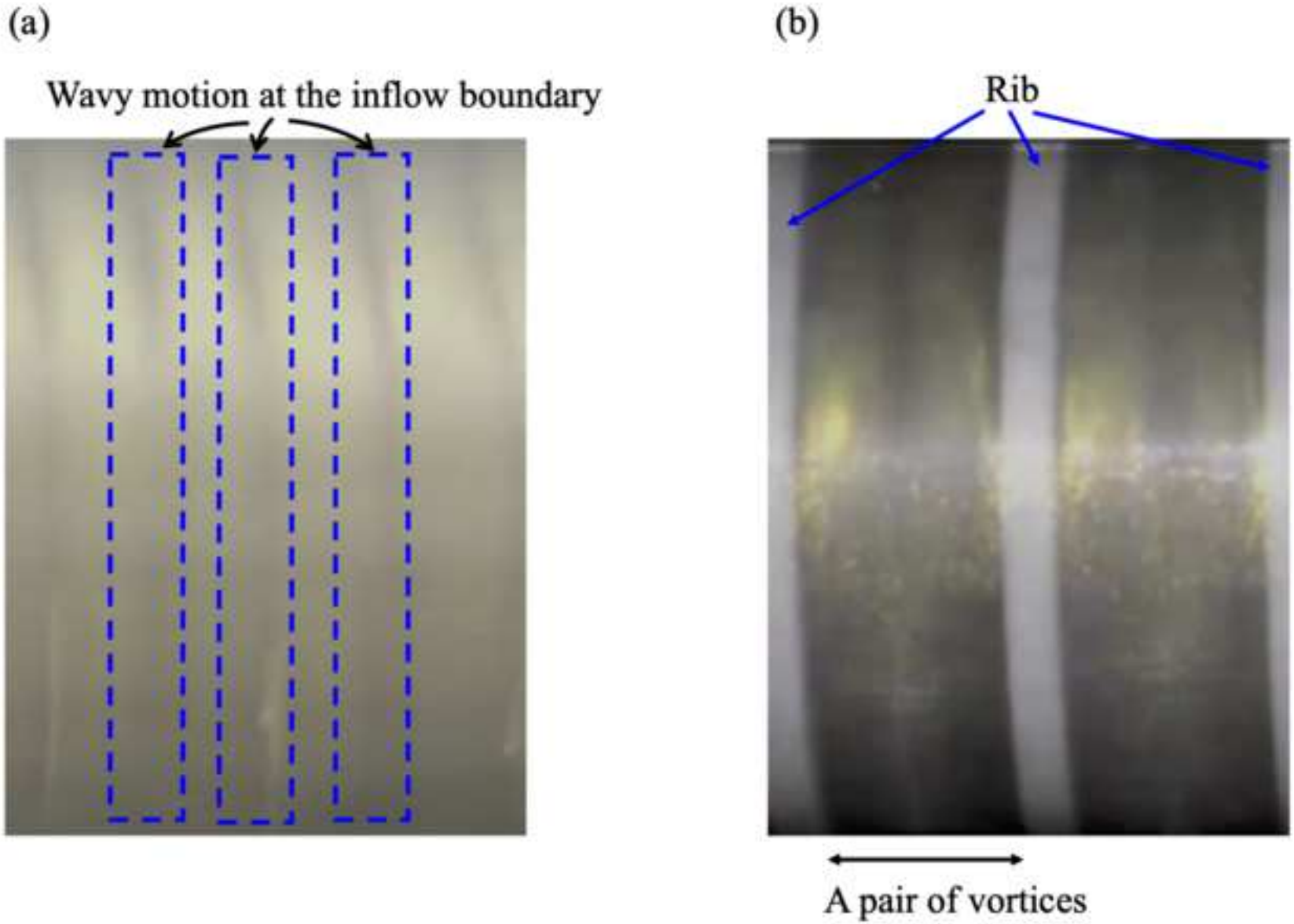

Figure7
Click here to download high resolution image

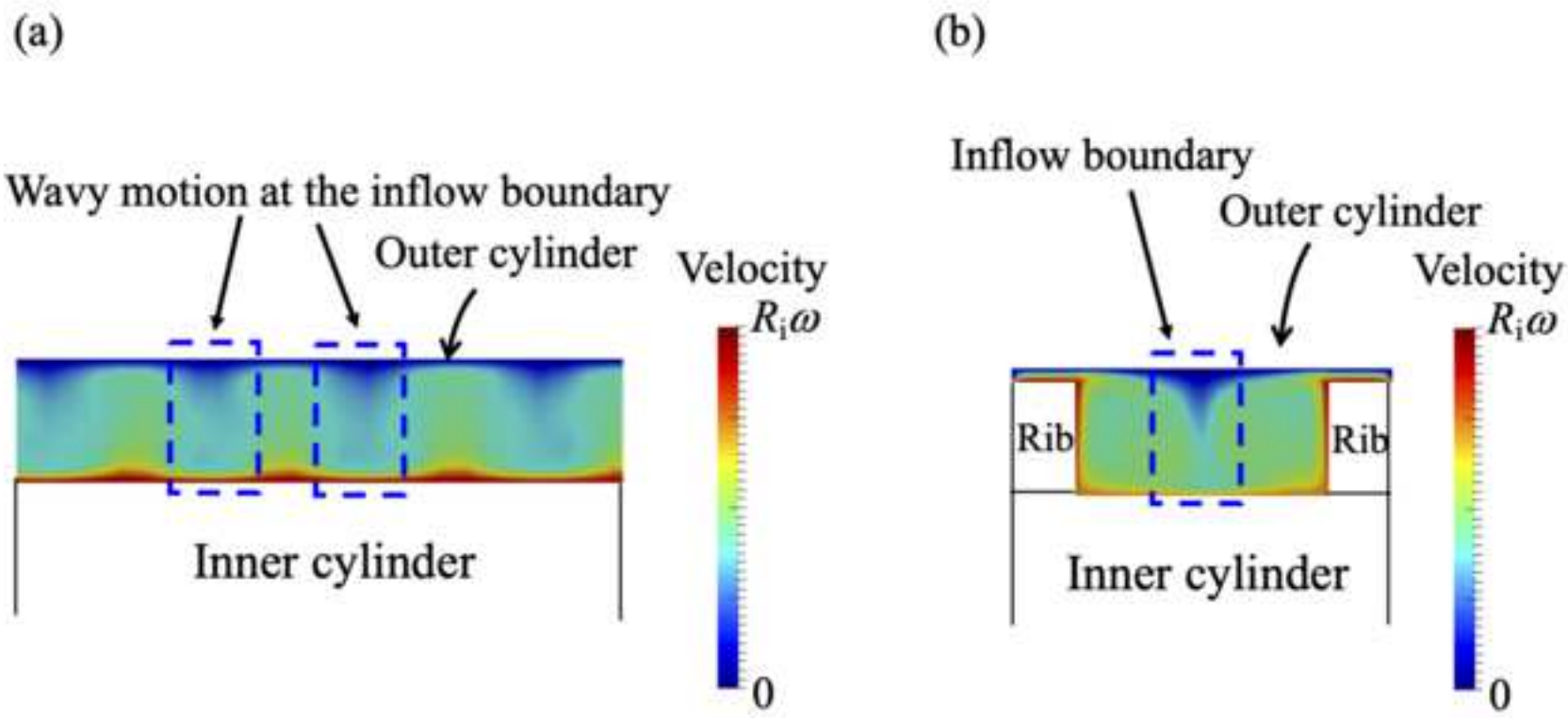

Figure8
Click here to download high resolution image

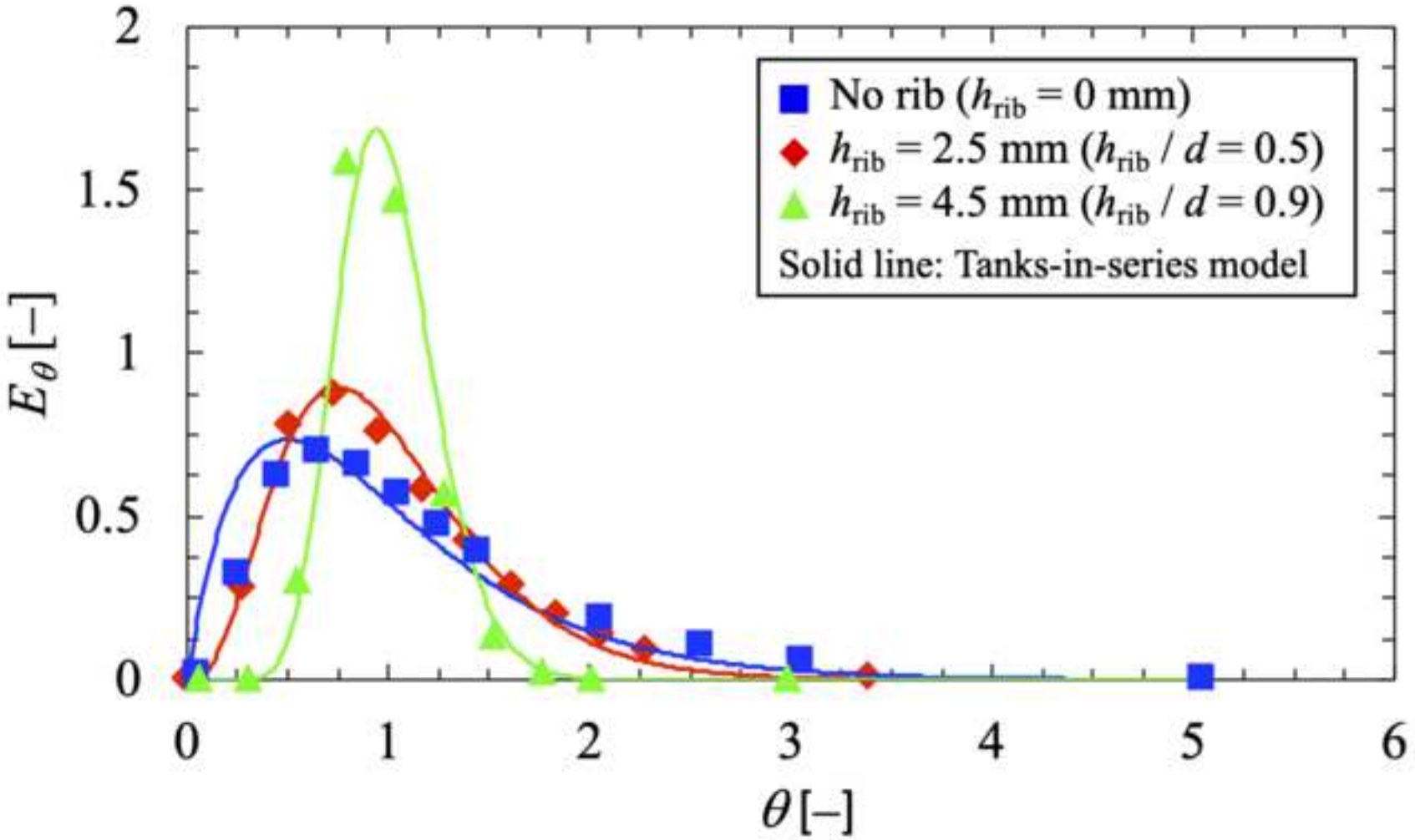

Figure9
Click here to download high resolution image

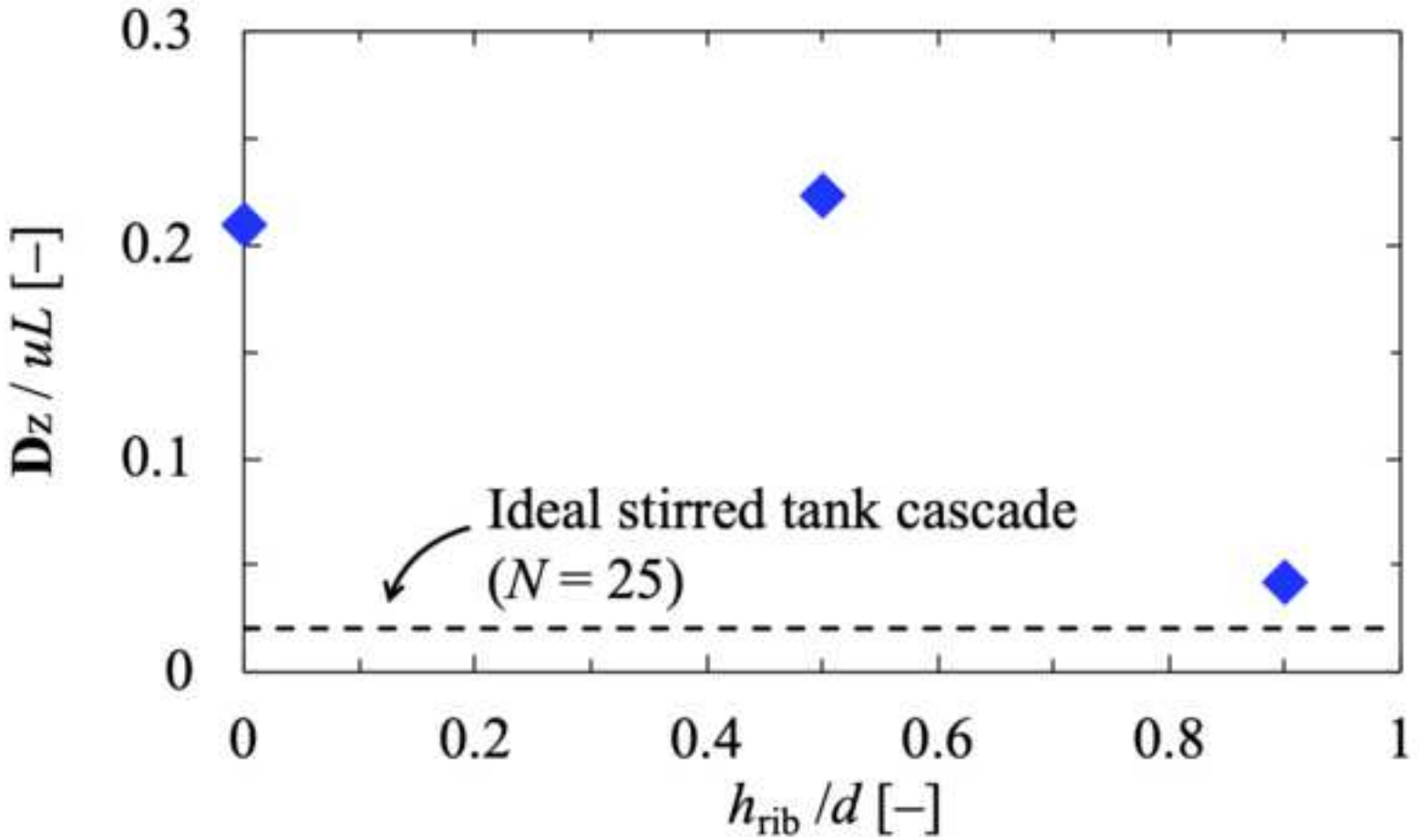

Figure10
Click here to download high resolution image

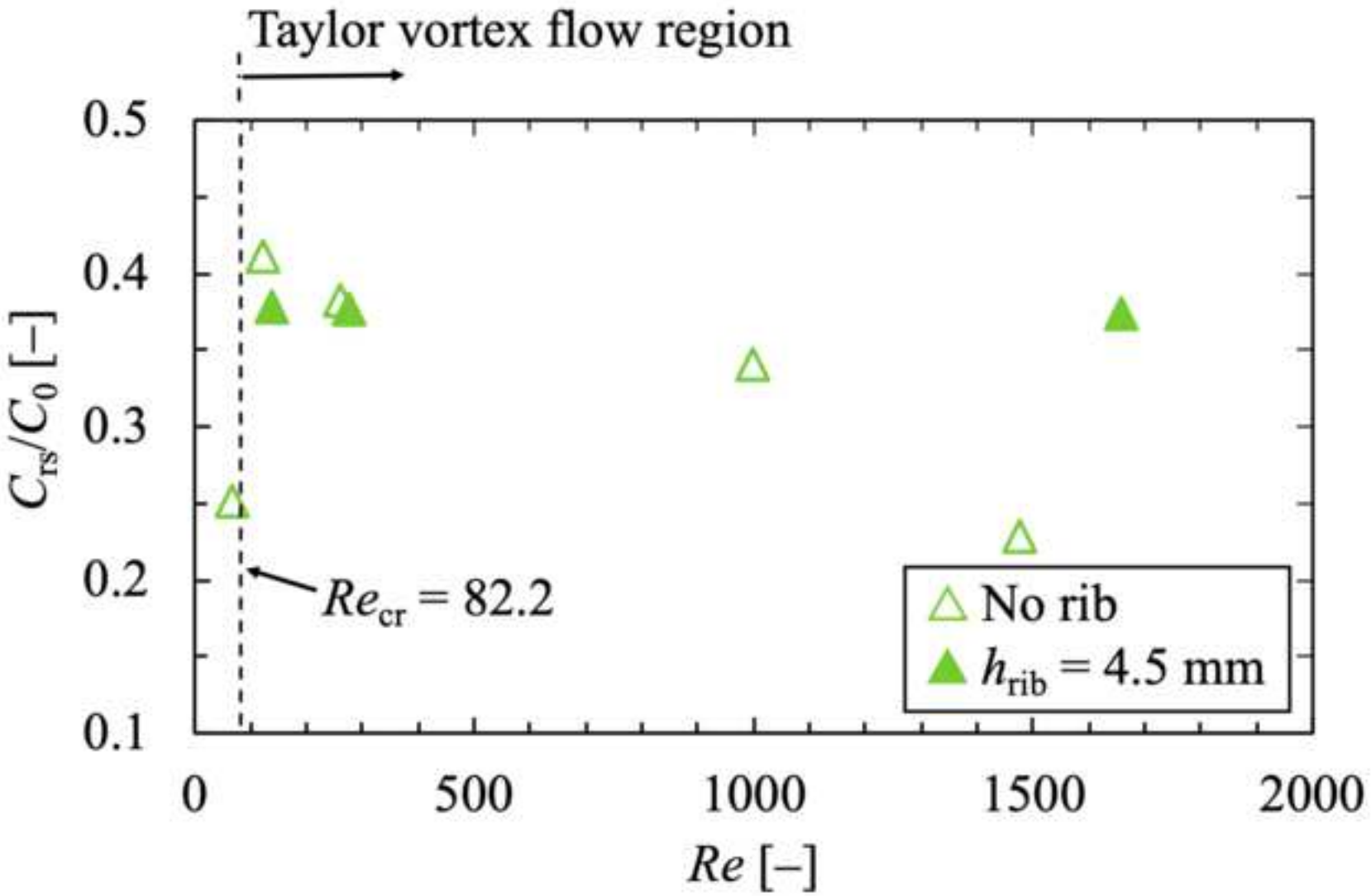

Figure11
Click here to download high resolution image

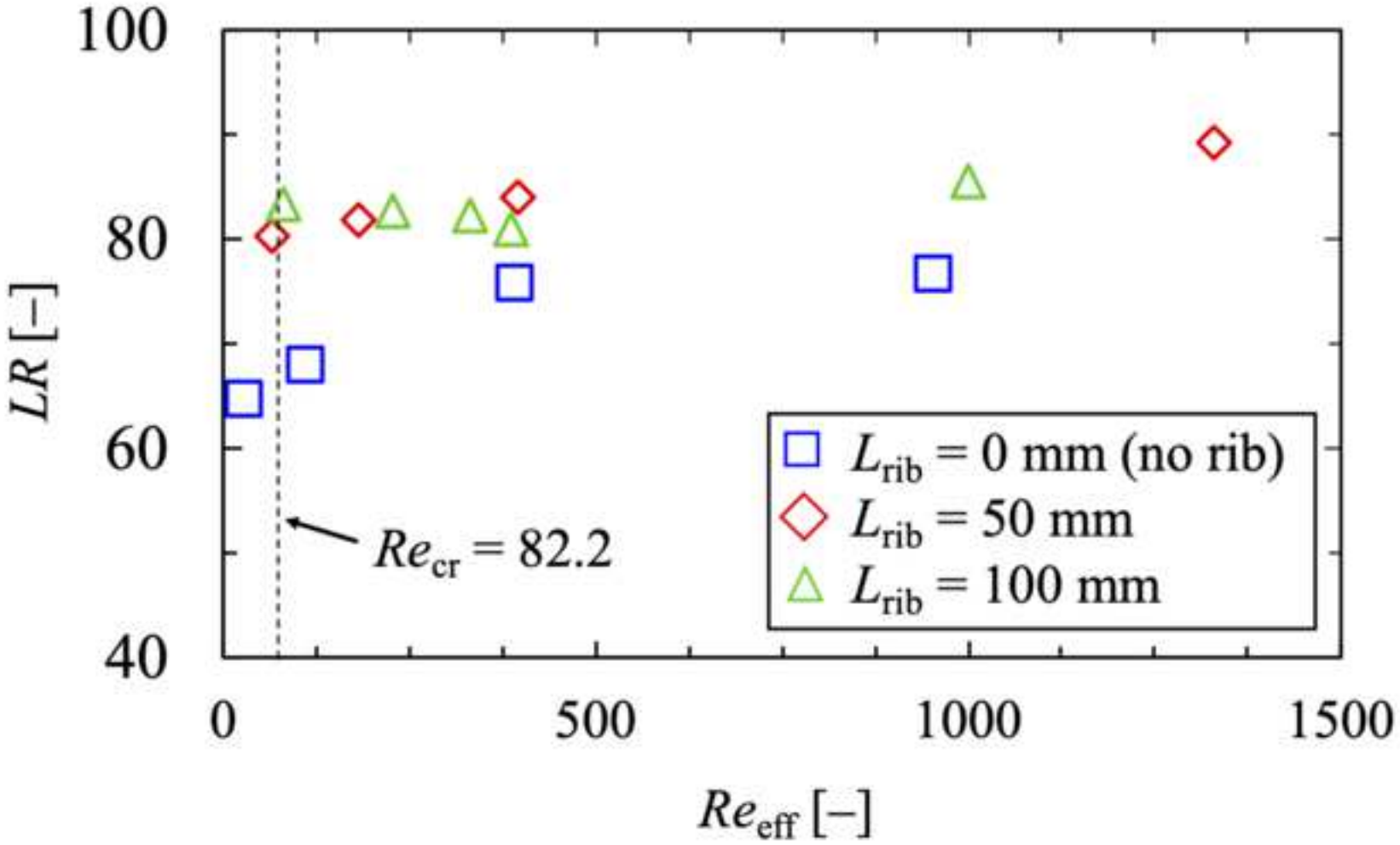

Figure12
Click here to download high resolution image

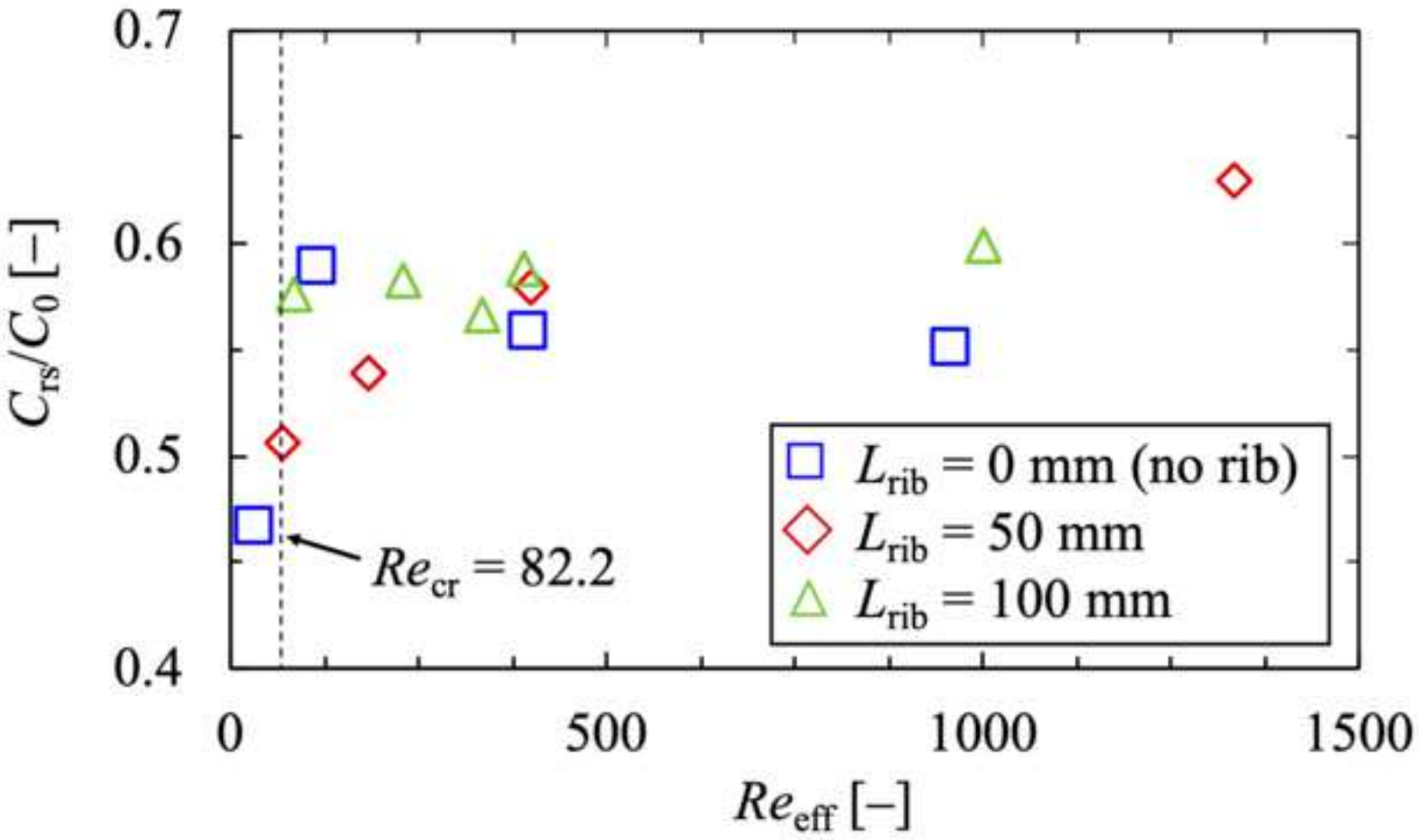

Figure13
Click here to download high resolution image